Ultrasonic Absorption and Relaxation Phenomena in Molten Nitrate Mixtures

J. Richter and B. Fuchs
Institut für Physikalische Chemie der RWTH Aachen, Aachen

Z. Naturforsch. **41 a**, 535–544 (1986); received November 25, 1985

An optical device based on the Debye-Sears effect is developed to determine the ultrasonic absorption and velocity in molten alkali nitrate + silver nitrat mixtures. $RbNO_3 + AgNO_3$ and $CsNO_3 + AgNO_3$ are investigated in the total composition range between 480 K and 580 K within a frequency interval from 10 MHz to 35 MHz. In the concentration range of high ultrasonic absorption we find dispersion and a frequency dependent step in the absorption curve caused by relaxation. The relaxation time of the structural relaxation in the molten salt mixtures investigated here is in the order of 10^{-8} s.

The volume viscosity, the adiabatic constant, and the compressibilities are calculated.

1. Introduction

In a previous paper [1] we used the pulse transmission method to determine the ultrasonic velocity and absorption in nitrate melts, where the loss of intensity is recorded as a function of the distance between transmitter and receiver. Because of the relatively low absorption in the ultrasonic region up to 35 MHz the parasitic absorptions dominate to such an extend that absorption measurements can only be performed with an accuracy of about 10%, whereas measurements of the ultrasonic velocity are possible with a high precision.

To enable more precision measurements of ultrasonic absorptions in molten salts, we adapted the Debye-Sears method [2] to liquids at higher temperatures and applied it to nitrate melts.

2. Experimental

An ultrasonic wave generates dilatation and compression zones in a melt which appear as a phase lattice to a laser beam perpendicular to the sound wave. The diffraction of light by a propagating sound wave equals the diffraction by a lattice moving at the velocity of sound. As the ultrasonic velocity is small against the velocity of light, the movement of the sound lattice does not affect the intensity distribution over the diffraction orders. For low sound intensities, i.e. in the area of linear acoustics, and with the assumption that the intensities of the two first diffraction orders are very small compared to that of zeroth order, Born [3] showed that there is a proportionality between the intensities of sound and light. But this relation only holds if no other density variations, except the ones induced by the sound wave, are generated. According to Wagner [4] only the two first orders appear beside the zero order, if a sine-shaped sound wave is applied. This is a necessary condition for the proportionality between the sound and light intensities.

The experimental set-up is shown in Figure 1. The light source is a He-Ne-laser of 7 mW continuous output and a wavelength of 632.8 nm. For the measurement of the ultrasonic velocity a camera with winder, databack, and view finder is used. The diffraction pattern is recorded on a black and white film Agfapan 25 S and is analyzed with a measuring microscope, the table of which can be positioned in x- and y-direction with an accuracy of 1 µm.

For the ultrasonic absorption measurements a photocell is placed into the first order beam. After amplification the photo current is recorded by a digital multimeter and transferred to a calculator and printer via an interface.

At the bottom of the cell a sound absorber avoids disturbances of the measurement by reflected sound waves. Thus it is guaranteed that the measurement is carried out in a field of a propagating ultrasonic wave, whereas in a field of stationary waves the energy density would be periodically depending on

Reprint requests to Prof. Dr. J. Richter, Institut für Physikalische Chemie der RWTH Aachen, Templergraben 59, D-5100 Aachen.

0340-4811 / 86 / 0300-0535 $ 01.30/0. – Please order a reprint rather than making your own copy.

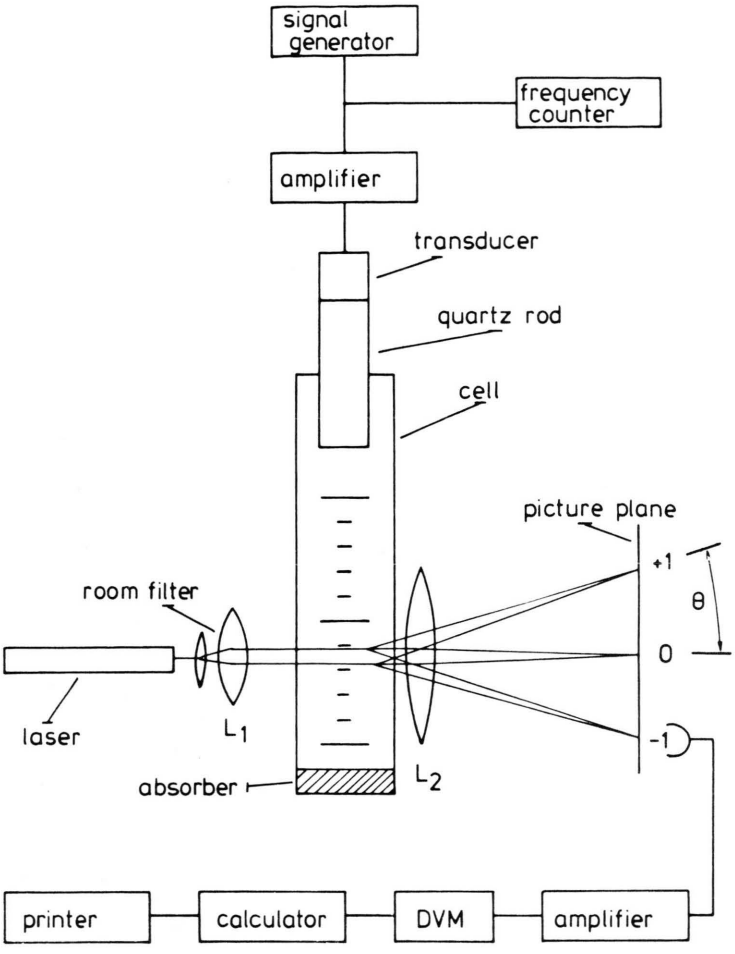

Fig. 1. Experimental set-up of the Debye-Sears method.

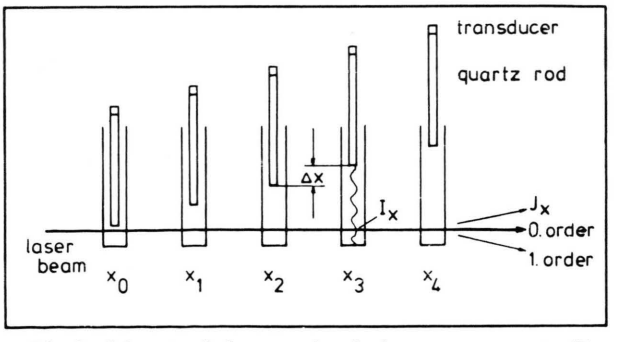

Fig. 2. Scheme of the sound velocity measurements (I_x: sound intensity, J_x: light intensity).

position rather than decreasing exponentially, and therefore an absorption measurement would not be feasible.

In order to generate the ultrasonic waves, the electrical vibration produced by a signal generator (Hewlett Packard, type 8640B), is amplified, and transmitted to electroacoustic transducers (piezoelectric effect) with resonance frequencies between 10 MHz and 35 MHz. Since the transducers, because of their piezoelectric properties, are temperature sensitive, the sound wave must be coupled into the melt via a quartz rod. The distance between laser beam and quartz rod is adjusted with a micromanipulator, which varies the immersion depth with a repetition accuracy of 5 μm (10% of the ultrasonic wave length).

At a distance x of the laser beam from the end of the quartz rod the ultrasonic intensity is attenuated by the melt and, accordingly, the intensity of the laser light diffracted into the first order is

$$J_x = J_0 \exp(-2\alpha x) . \tag{1}$$

J_x denotes the light intensity at position x, J_0 at position $x = 0$ and α the absorption coefficient.

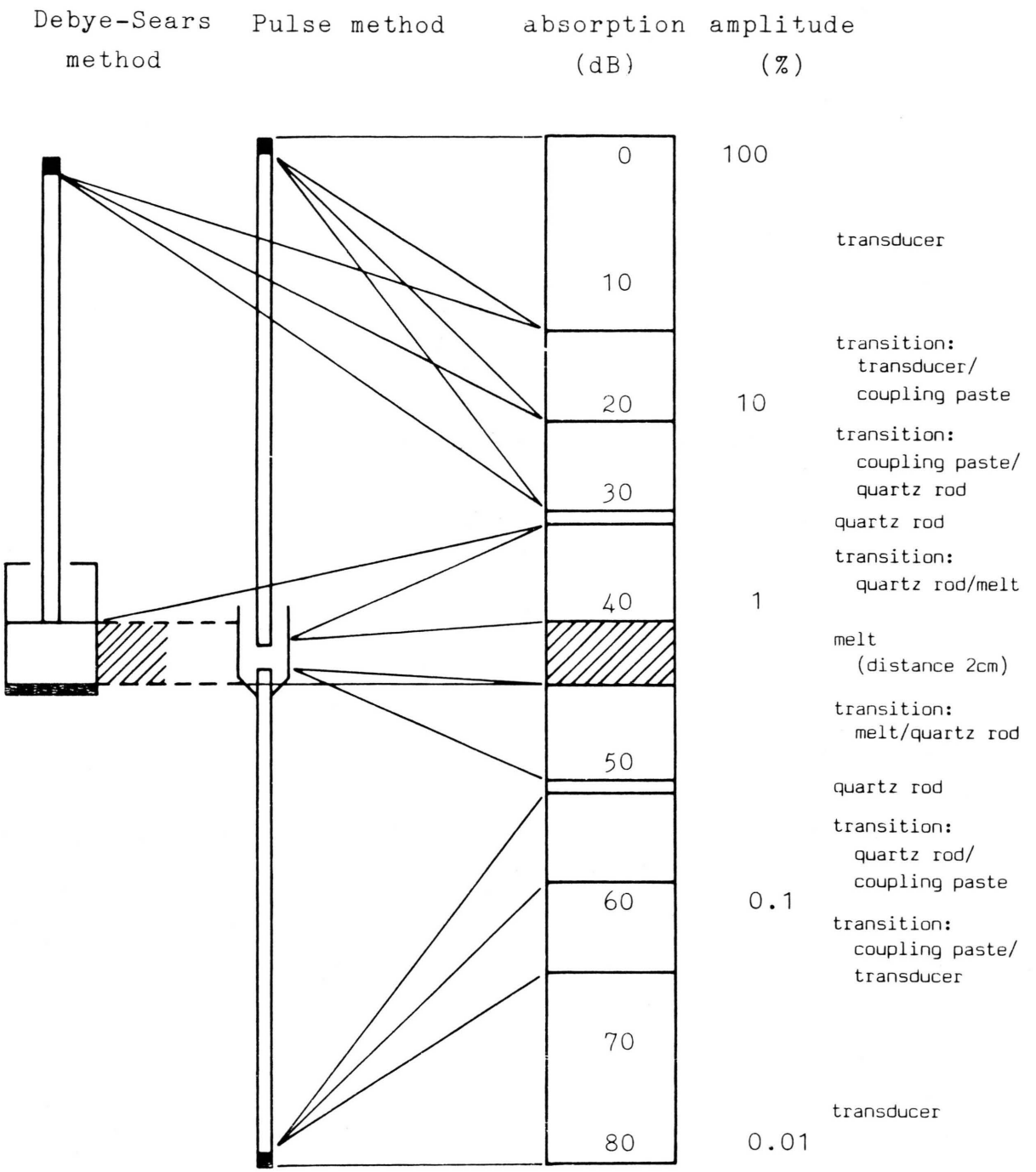

Fig. 3. Sound absorption in the different parts of the experimental set-up of the Debye-Sears method (left) and pulse method (centre).

The resulting photo current variation is in the order of some nA. It is transformed into a proportional voltage and amplified:

$$\ln U_x = -2\alpha x + \ln U_0 \tag{2}$$

(U_x, U_0: Voltage at positions x and $x = 0$). The quartz rod is moved up in five steps, 4 mm each, as shown in Figure 2.

In order to be able to perform absorption measurements in an unobjectionable sound field, the length of the quartz rod has to be longer than the range of the stray in which reflections at the glass surface result in strong echos. An undisturbed sound field is ensured with a length of the quartz rod of 350 mm at 10 mm diameter.

The measurement cell is made of stainless steel with optical passages. At temperatures above 350 °C (because of sealing problems) a Suprasil quartz cell is used. For further experimental details see [5].

The parasitic absorptions, in comparison to the pulse transmission method [1], are reduced by 40 dB according to Fig. 3, that is by a factor 100 in amplitude.

The ultrasonic velocity u is calculated according to

$$u = \frac{\lambda f A}{a}, \tag{3}$$

where λ stands for the light wave length, f for the ultrasonic frequency, A for the focal distance of lens L_2, and a for the distance between zero and first diffraction order in the image plane (s. Fig. 1) that has to be measured.

The apparatus, based on the concept of Lucas and Biquard [6], was tested by performing measurements on water. The measured values of the absorption coefficient were in good agreement with those of Davies [7], Litovitz [8], and Hawley [9].

The velocity values agree well with those of Willard [10]. Further we could use the measurements on water to prove that the distance a is nearly independent of the distance between ultrasonic lattice and imaging lens L_2. This shows that lens L_2 may be placed outside the furnace without a negative influence on the measurements.

3. Results

In the following we discuss the results on sound absorption in terms of αf^{-2}, because this expression, like the ultrasonic velocity u, is independent of frequency over broad frequency ranges. Moreover, where αf^{-2} does dependent on frequency, its frequency dependence resembles that of u.

The error bars in the figures correspond to a confidence interval of 95%, i.e. an interval of 2σ.

Table 1. $RbNO_3 + AgNO_3$: Ultrasonic absorption, velocity, density, shear viscosity, and volume viscosity at 25 MHz as functions of the mole fraction x_2 of $AgNO_3$.

x_2	T / K	$\alpha f^{-2} \cdot 10^{15}$ / $s^2\,m^{-1}$	u / $m\,s^{-1}$	ϱ / $kg\,m^{-3}$	$\eta \cdot 10^3$ / $kg\,s^{-1}\,m^{-1}$	$\alpha_{class} f^{-2} \cdot 10^{15}$ / $s^2\,m^{-1}$	α / α_{class}	$\eta_v \cdot 10^3$ / $kg\,s^{-1}\,m^{-1}$	η_v / η
0.00	620	120	1444	2488	3.20	11.24	10.67	41.27	13.0
0.20	580	89	1453	2722	3.45	8.18	10.00	33.05	9.6
	510	106	1535	2802	5.32	14.15	7.49	46.06	8.7
0.30	580	99	1436	2832	3.26	10.23	9.68	37.71	11.6
0.40	580	92	1425	2952	3.07	9.46	9.73	35.72	11.6
	540	100	1466	3000	3.85	10.72	9.33	42.75	11.1
	480	112	1535	3073	5.81	13.76	8.14	55.32	9.5
0.50	580	63	1435	3080	2.94	8.50	7.35	24.90	8.5
0.60	580	43	1425	3218	2.76	7.80	5.51	16.61	6.0
	540	50	1470	3267	3.54	9.00	5.57	21.57	6.1
	510	55	1505	3303	4.28	10.00	5.50	25.66	6.0
	480	54	1542	3340	5.30	11.39	4.74	26.44	5.0
	430	90	1593	3400	8.08	15.47	5.82	51.89	6.4
0.70	580	39	1418	3365	2.77	7.60	5.13	15.26	5.5
0.80	580	36	1436	3522	2.74	6.92	5.21	13.37	5.6
1.00	580	27	1483	3853	2.75	5.76	4.69	13.52	4.9

Table 2. $CsNO_3 + AgNO_3$: Ultrasonic absorption, velocity, density, shear viscosity, and volume viscosity as functions of the composition at 25 MHz.

x_2	T / K	$\alpha f^{-2} \cdot 10^{15}$ / $s^2\,m^{-1}$	u / $m\,s^{-1}$	ϱ / $kg\,m^{-3}$	$\eta \cdot 10^3$ / $kg\,s^{-1}\,m^{-1}$	$\alpha_{class} f^{-2} \cdot 10^{15}$ / $s^2\,m^{-1}$	α / α_{class}	$\eta_v \cdot 10^3$ / $kg\,s^{-1}\,m^{-1}$	η_v / η
0.00	720	395	1203	2773	2.05	11.2	35.3	93.8	45.8
0.35	580	112	1298	3170	3.15	12.0	9.4	35.1	11.2
0.40	580	77	1299	3211	3.10	11.6	6.6	23.3	7.5
0.50	580	74	1321	3293	3.00	10.4	7.1	24.3	8.1
0.55	580	95	1326	3327	3.00	10.2	9.3	33.3	11.1
0.65	580	117	1347	3421	2.91	9.1	12.8	45.9	15.8
	540	125	1390	3477	3.71	10.5	12.0	54.2	14.6
	490	106	1444	3540	5.32	13.1	8.9	50.1	9.4
0.70	580	91	1350	3483	2.87	8.8	10.3	35.7	12.4
0.80	580	56	1373	3596	2.80	7.9	7.1	22.8	8.2
0.90	580	45	1393	3710	2.75	7.2	6.2	19.2	7.0
1.00	580	27	1483	3853	2.75	5.8	4.7	13.5	4.9

Table 3. $RbNO_3 + AgNO_3$: Ultrasonic absorption and velocity at different frequencies and 580 K. $CsNO_3 + AgNO_3$: Ultrasonic absorption at different frequencies and temperatures in the composition range of maximum absorption.

$RbNO_3 + AgNO_3$					$CsNO_3 + AgNO_3$			
x_2	T / K	f / MHz	$\alpha f^{-2} \cdot 10^{15}$ / $s^2\,m^{-1}$	u / $m\,s^{-1}$	x_2	T / K	f / MHz	$\alpha f^{-2} \cdot 10^{15}$ / $s^2\,m^{-1}$
0.2	580	16.302	117	–	0.65	580	15.197	179
		25.340	89	–			25.514	117
		31.689	71	–			26.594	77
							30.853	54
0.3	580	23.742	280	–				
		25.368	–	–		540	15.454	145
		30.544	142	–			18.756	136
		34.113	73	–			25.813	125
							31.671	78
0.5	580	9.085	280	1320				
		15.680	206	1333		490	15.849	119
		25.860	63	1435			19.204	116
		33.695	66	1428			25.719	106
							29.153	93
							30.709	79

Ultrasonic absorption

The ultrasonic absorption as a function of mole fraction of silver nitrate x_2 at different temperatures and at 25 MHz is listed in Table 1 for the system $RbNO_3 + AgNO_3$, and in Table 2 for the system $CsNO_3 + AgNO_3$. In Fig. 4 αf^{-2} is plotted against x_2 for both systems at 580 K and 25 MHz. The αf^{-2}-values for the system $KNO_3 + AgNO_3$ also measured with the Debye-Sears method, are plotted in the same Figure. They agree well with the values published in the previous paper [1], which were determined with the pulse transmission method. The values of the system $NaNO_3 + AgNO_3$ are also taken from [1].

All the investigated alkali nitrate–silver nitrate systems show a similar absorption behaviour. The maximum of the absorption curve is more pronounced for larger cations. The absolute values rise in the same sequence and the maximum value is shifted to the alkali nitrate side with the exception of $CsNO_3 + AgNO_3$, which has its maximum ab-

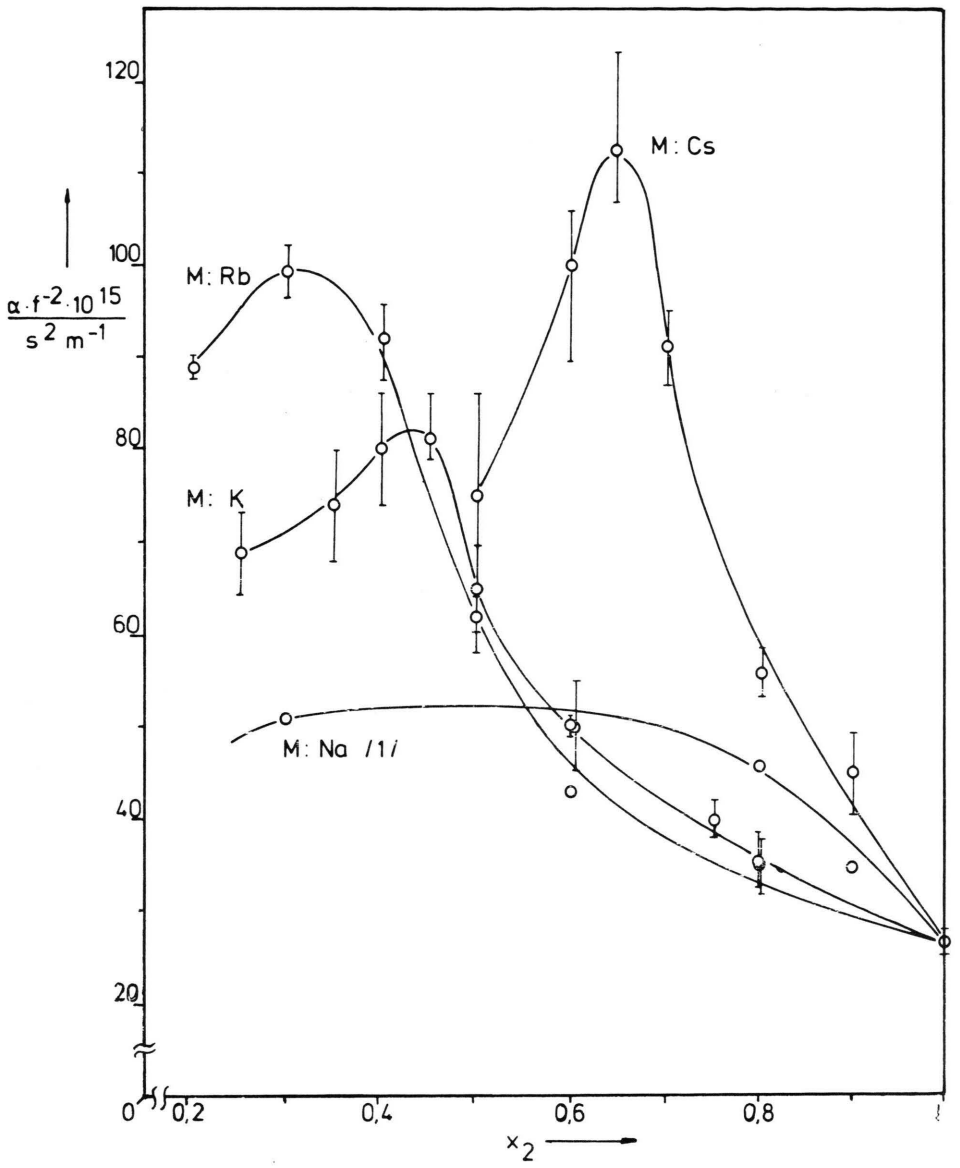

Fig. 4. (M)NO_3 + $AgNO_3$: Ultrasonic absorption as function of x_2, the mole fraction of $AgNO_3$ at $T = 580$ K and $f = 25$ MHz (M: Na, K, Rb, Cs).

sorption at $x_2 = 0.65$. The high absorption value listed in Table 2 at $x_2 = 0.35$ and $T = 580$ K is probably due to the fact that at this composition the measuring temperature is only 10 K above the melting point. The ultrasonic absorption rises exponentially with temperature in the region of the melting point, whereas 50 K above the melting point the absorption hardly depends on temperature [5].

The frequency dependences of the absorption for $RbNO_3 + AgNO_3$ and $CsNO_3 + AgNO_3$ in the composition range of maximum absorption are listed in Table 3. Figure 5 shows the almost completely measured step in the absorption versus frequency curve of $RbNO_3 + AgNO_3$ at $x_2 = 0.5$ and $T = 580$ K. The dashed line indicates that the absorption again becomes independent of frequency below 9 MHz,

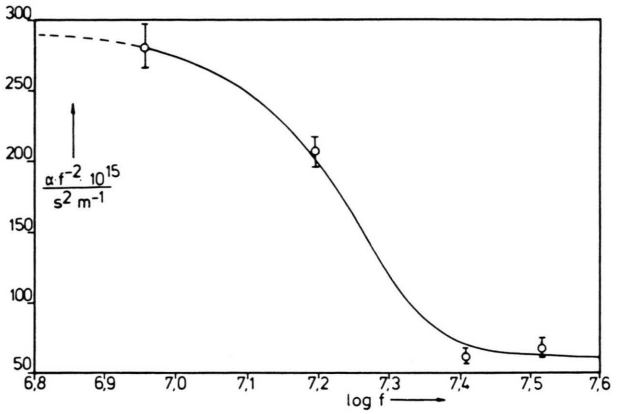

Fig. 5. $RbNO_3 + AgNO_3$: Ultrasonic absorption as function of the frequency at $x_2 = 0.5$ and $T = 580$ K.

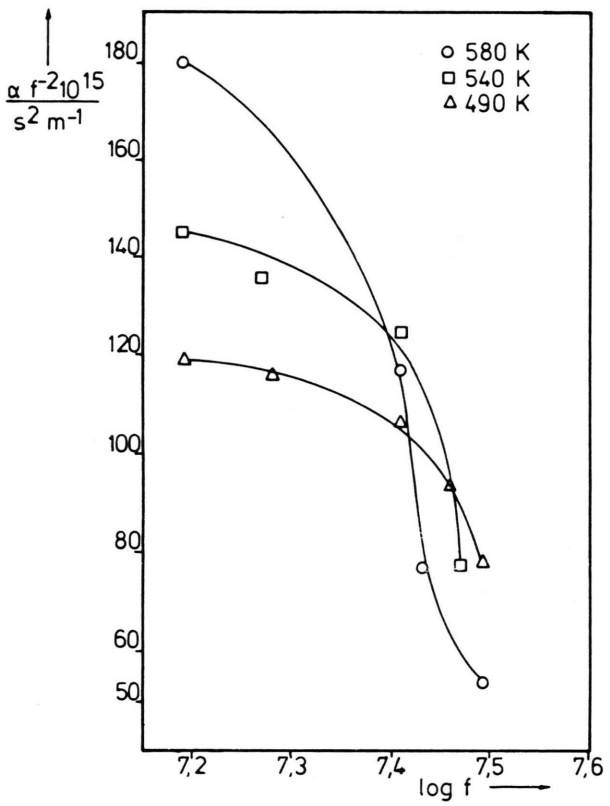

Fig. 6. $CsNO_3 + AgNO_3$: Ultrasonic absorption as function of the frequency at $x_2 = 0.65$ and three temperatures.

where we cannot measure the absorption. In Fig. 6 the steps for the system $CsNO_3 + AgNO_3$ are shown for three different temperatures and $x_2 = 0.65$. The high-frequency end of these steps were outside the frequency range of our experimental device.

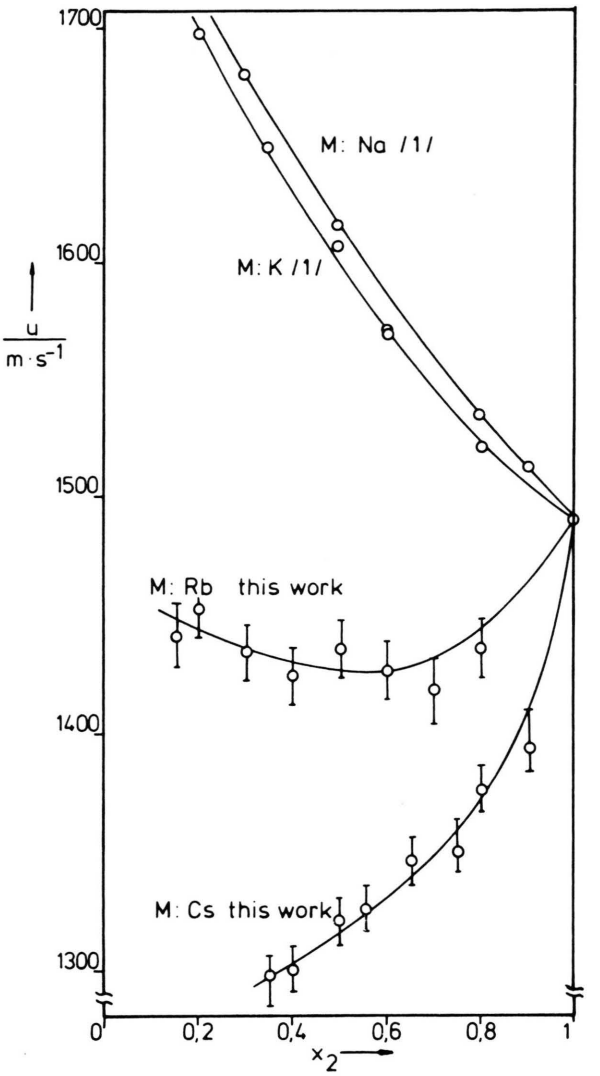

Fig. 7. $(M)NO_3 + AgNO_3$: Ultrasonic velocity as function of the composition at $T = 580$ K and $f = 25$ MHz (M: Na, K, Rb, Cs).

Ultrasonic velocity

In addition to the ultrasonic velocity measurements on $NaNO_3 + AgNO_3$ and $KNO_3 + AgNO_3$ in the previous paper [1] at 25 MHz, the systems $RbNO_3 + AgNO_3$ and $CsNO_3 + AgNO_3$ were measured with the Debye-Sears method in dependence on composition, temperature, and frequency. The results at 25 MHz are collected in Table 1 for $RbNO_3 + AgNO_3$ and in Table 2 for $CsNO_3 + AgNO_3$, both as a function of the composition at different temperatures. Figure 7 displays the con-

Table 4a. Balancing equation $u = a - bT$ for pure molten nitrates of different authors at different frequencies (sound velocity u in ms^{-1}, temperature T in °C).

Author	Torell and Knape [13]	Higgs and Litovitz [11]	Fuchs and Richter [1]	this work	Cerisier et al. [12]	Moret [14]
f	10 GHz	100 MHz	28 MHz	25 MHz	0.1 MHz	0.1 MHz
$RbNO_3$	$1917 - 1.10\,T$			$1857 - 1.18\,T$		
$CsNO_3$	$1645 - 0.93\,T$			$1720 - 1.15\,T$		$1645 - 1.025\,T$
$AgNO_3$	$1850 - 0.97\,T$	$1790 - 0.873\,T$	$1876 - 1.25\,T$	$1863 - 1.23\,T$	$1915.6 - 1.8083\,T + 16.2024 \cdot 10^{-4}\,T^2$	

Table 4b. Coefficients of the balancing equation $u = a - bT$ for $RbNO_3 + AgNO_3$ and $CsNO_3 + AgNO_3$ as functions of the composition at 25 MHz.

	$RbNO_3 + AgNO_3$		$CsNO_3 + AgNO_3$	
x_2	a / ms^{-1}	b / $ms^{-1}K^{-1}$	a / ms^{-1}	b / $ms^{-1}K^{-1}$
0.0	2127	1.18	1990	1.15
0.2	2132	1.18	–	–
0.3	2132	1.20	–	–
0.4	2098	1.16	–	–
0.55	–	–	1910	1.00
0.6	2075	1.12	–	–
0.65	–	–	2014	1.15
0.7	2073	1.13	–	–
0.8	2004	0.98	2031	1.13
1.0	2196	1.23	–	–

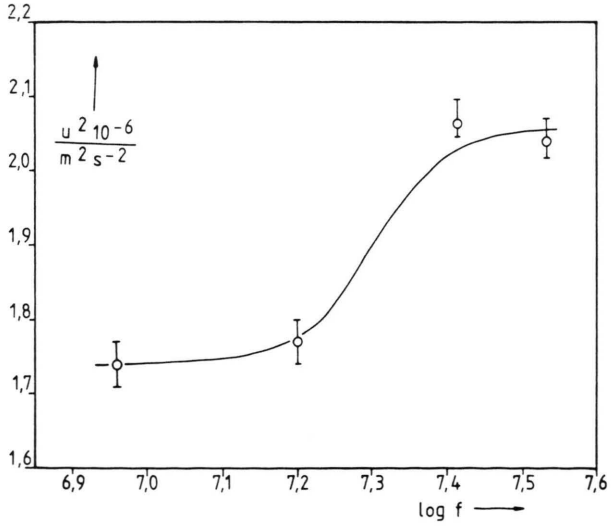

Fig. 8. $RbNO_3 + AgNO_3$: Sound velocity as function of the frequency at $x_2 = 0.5$ and $T = 580$ K.

centration dependence of all four systems at 580 K and 25 MHz.

The linear temperature dependences of the velocity of sound for the pure nitrates measured by different authors are collected in Table 4a for different frequencies. The corresponding concentration dependent constants of the mixtures measured in this work are listed in Table 4b.

The results of our frequency dependent velocity measurements on $RbNO_3 + AgNO_3$ and $CsNO_3 + AgNO_3$ show that dispersion is observable at 580 K. The velocity is nearly frequency independent for frequencies up to 28 MHz. To higher frequencies it rises steeply. Our device does not allow to measure at frequencies higher than 35 MHz. An exception is again $RbNO_3 + AgNO_3$ at $x_2 = 0.5$ (Figure 8). For this system the dispersion step already occurs between 15 and 25 MHz.

Volume viscosity and thermodynamic properties

The volume viscosity η_v is calculated according to [1]:

$$\frac{\eta_v}{\eta} = \left(\frac{3}{4}\,\frac{\alpha}{\alpha_{class}} - 1\right). \tag{4}$$

The classic absorption coefficient α_{class} is calculated with the measured ultrasonic velocity values and the literature values for density ϱ and shear viscosity η [15]. The volume viscosity and the other associated data, as well as the ratios α/α_{class} and η_v/η are listed in Table 1 for $RbNO_3 + AgNO_3$ and in Table 2 for $CsNO_3 + AgNO_3$. A comparison of η_v with the ultrasonic absorption shows that the concentration dependence of the absorption is mainly due to the volume viscosity and consequently to relaxation processes.

Table 5. Expansion coefficient, heat capacity, adiabatic constant, and compressibilities as functions of the composition at 25 MHz.

x_2	T / K	$\alpha_V \cdot 10^4$ / K^{-1}	$\tilde{C}_P$ / $J\,kg^{-1}\,K^{-1}$	γ	$\chi_T \cdot 10^{10}$ / $s^2\,m\,kg^{-1}$	$\chi_s \cdot 10^{10}$ / $s^2\,m\,kg^{-1}$
0.0	650	4.52	1210	1.217	2.511	2.064
	620	4.46		1.213	2.338	1.928
	600	4.42		1.210	2.230	1.844
0.2	580	4.19	1132	1.190	2.070	1.740
	510	4.07		1.176	1.781	1.515
0.3	580	4.20	1093	1.193	2.043	1.710
	450	3.99		1.166	1.540	1.320
0.4	580	4.10	1055	1.188	1.981	1.670
	540	4.03		1.179	1.829	1.550
	480	3.94		1.166	1.611	1.380
	430	3.86		1.155	1.442	1.250
0.5	580	3.96	1015	1.185	1.868	1.577
0.6	580	3.76	976	1.171	1.791	1.530
	540	3.70		1.164	1.649	1.420
	510	3.66		1.159	1.549	1.340
	480	3.62		1.154	1.452	1.260
	430	3.36		1.140	1.323	1.160
0.7	580	3.57	938	1.158	1.712	1.478
	540	3.52		1.152	1.583	1.375
	510	3.48		1.147	1.488	1.297
	480	3.44		1.143	1.400	1.221
0.8	580	3.29	898	1.145	1.576	1.377
	540	3.25		1.138	1.468	1.290
	510	3.22		1.133	1.386	1.224
1.0	620	2.94	819	1.135	1.451	1.279
	580	2.91		1.131	1.335	1.180
	540	2.86		1.126	1.227	1.090

Table 6. $CsNO_3 + AgNO_3$: Expansion coefficient, heat capacity, adiabatic constant, and compressibilities as functions of the composition at 25 MHz.

x_2	T / K	$\alpha_V \cdot 10^4$ / K^{-1}	$\tilde{C}_P$ / $J\,kg^{-1}\,K^{-1}$	γ	$\chi_T \cdot 10^{10}$ / $s^2\,m\,kg^{-1}$	$\chi_s \cdot 10^{10}$ / $s^2\,m\,kg^{-1}$
0.00	750	4.38	974	1.201	3.233	2.692
	720	4.33		1.200	2.991	2.492
	700	4.30		1.198	2.885	2.408
0.35	580	3.79	920	1.152	2.157	1.872
0.40	580	3.74	913	1.150	2.122	1.845
0.50	580	3.64	897	1.150	2.001	1.740
0.55	580	3.61	890	1.149	1.964	1.710
	540	3.55		1.143	1.807	1.581
	510	3.51		1.140	1.701	1.494
	480	3.48		1.134	1.615	1.426
0.65	580	3.51	874	1.148	1.850	1.611
	540	3.45		1.145	1.700	1.489
	490	3.39		1.142	1.537	1.355
	450	3.35		1.134	1.404	1.243
0.70	580	3.45	866	1.145	1.804	1.575
0.80	580	3.34	853	1.143	1.679	1.469
	540	3.29		1.140	1.510	1.322
	510	3.26		1.133	1.463	1.291
	480	3.23		1.130	1.371	1.213
0.90	580	3.24	835	1.141	1.585	1.389
1.00	580	2.91	819	1.132	1.335	1.180

The adiabatic constant γ, the expansion coefficient α_v, the adiabatic compressibility χ_s, and the resulting isothermal compressibility χ_T are calculated according to Eqs. (5)–(8) of [1] from the ultrasonic velocities measured here, the temperature dependent densities of Brillant [16], and the specific heat capacities of the pure salts of Gustafsson [17] and Janz [18], assuming a linear dependence on composition. All calculated values of the systems $RbNO_3 + AgNO_3$ and $CsNO_3 + AgNO_3$ are listed in Table 5 and 6.

4. Conclusions

Two mechanisms for ultrasonic absorption are being discussed, which are based on the shear and volume viscosity, respectively. The latter can often be attributed to a relaxation process. In the previous paper [1] we could conclude from comparisons with absorption curves of water–alcohol mixtures that "structural relaxation" prevails in the case of nitrate melts. This conclusion is supported by the results of this work.

The differing concentration dependences of the ultrasonic velocities of the nitrate melts (Fig. 7) also hint to structural changes with increasing cation radius, as well as the observation that the ultrasonic velocity is frequency dependent only in the system with larger cations: $RbNO_3 + AgNO_3$ and $CsNO_3 + AgNO_3$. The frequency dependence becomes very pronounced in mixtures with strongest absorption.

In the Kneser theory of relaxation [18] the relaxation time is linked to the dispersion step of the sound velocity and the inflection point of the frequency dependent sound absorption curve. In general the relaxation time of the velocity is slightly smaller than the one of the absorption.

From our graphs we get the following relaxation times for the system $RbNO_3 + AgNO_3$ at $x_2 = 0.5$ and $T = 580\,K$

$$\tau = \frac{1}{2\pi f} = 10^{-8}\,s \quad \text{from the absorption curve (Fig. 5),}$$

$$\tau = \frac{1}{2\pi f} = 7 \cdot 10^{-9}\,s \quad \text{from the dispersion curve (Figure 8).}$$

Acknowledgement

We thank the Bundesminister für Forschung und Technologie (BMFT), Bonn, and the Fonds der Chemischen Industrie for financial support of this work.

[1] W. Fuchs and J. Richter, Z. Naturforsch. **39a,** 1279 (1984).
[2] P. Debye and F. Sears, Proc. Nat. Acad. Sci. Washington **18,** 409 (1932).
[3] M. Born and E. Wolf, Principles of Optics, Pergamon Press, Rochester 1980.
[4] E. H. Wagner, Z. Physik **141,** 604 (1955).
[5] B. Fuchs, Thesis Aachen 1985.
[6] R. Lucas and P. Biquard, J. Phys. **10,** 464 (1932).
[7] C. M. Davies and J. Jarzynski, Final Report Office of Saline Water Grant No. 14-01-0001-684 (1968).
[8] T. A. Litovitz and E. H. Carnevale, J. Appl. Phys. **26,** 816 (1955).
[9] S. Hawley, J. Allegra, and G. Holton, J. Acoust. Soc. Amer. **47,** 137 (1970).
[10] G. Willard, J. Acoust. Soc. Amer. **12,** 438 (1941).
[11] R. W. Higgs and T. A. Litovitz, J. Acoust. Soc. Amer. **32,** 1108 (1960).
[12] P. Cerisier, G. Finiels, and Y. Doucet, J. Chim. Phys. **71,** 836 (1974).
[13] H. E. Knape and L. M. Torell, Z. Naturforsch. **32a,** 57 (1977).
[14] J. M. Moret, Thesis, Marseille 1975.
[15] G. J. Janz, U. Krebs, H. F. Siegenthaler, and R. P. T. Tomkins, J. Phys. Chem. Ref. Data **1,** 581 (1972).
[16] S. Brillant, J. Chim. Phys. **65,** 2138 (1968).
[17] S. E. Gustafsson, N. O. Halling, and R. A. E. Kjellander, Z. Naturforsch. **23a,** 44, 682 (1968).
[18] H. O. Kneser, Ergebn. exakt. Naturwiss. **22,** 121 (1949).